J Nanopart Res (2018) 20: 11
https://doi.org/10.1007/s11051-017-4103-4

RESEARCH PAPER

Interfacial engineering of CuO nanorod/ZnO nanowire hybrid nanostructure photoanode in dye-sensitized solar cell

Bayram Kilic · Sunay Turkdogan · Aykut Astam · Sümeyra Seniha Baran · Mansur Asgin · Emre Gur · Yusuf Kocak

Received: 27 July 2017 / Accepted: 8 December 2017 / Published online: 7 January 2018

Abstract Developing efficient and cost-effective photoanode plays a vital role determining the photocurrent and photovoltage in dye-sensitized solar cells (DSSCs). Here, we demonstrate DSSCs that achieve relatively high power conversion efficiencies (PCEs) by using one-dimensional (1D) zinc oxide (ZnO) nanowires and copper (II) oxide (CuO) nanorods hybrid nanostructures. CuO nanorod-based thin films were prepared by hydrothermal method and used as a blocking layer on top of the ZnO nanowires' layer. The use of 1D ZnO nanowire/CuO nanorod hybrid nanostructures led to an exceptionally high photovoltaic performance of DSSCs with a remarkably high open-circuit voltage (0.764 V), short current density (14.76 mA/cm^2 under AM1.5G conditions), and relatively high solar to power conversion efficiency (6.18%) . The enhancement of the solar to power conversion efficiency can be explained in terms of the lag effect of the interfacial recombination dynamics of CuO nanorod-blocking layer on ZnO nanowires. This work shows more economically feasible method to bring down the cost of the nano-hybrid cells and promises for the growth of other important materials to further enhance the solar to power conversion efficiency.

Keywords Composite nanomaterials · CuO nanorods · ZnO nanowires · ZnO/CuO hybrid structures · Dye-sensitized solar cells · Interface engineering

B. Kilic (✉) · S. Turkdogan · S. S. Baran · M. Asgin
Department of Energy Systems Engineering, Faculty of Engineering, Yalova University, 77200 Yalova, Turkey
e-mail: bkilic@yalova.edu.tr
e-mail: kbayramkilic@gmail.com

A. Astam
Department of Physics, Faculty of Arts and Science, Erzincan University, 24100 Erzincan, Turkey

E. Gur · Y. Kocak
Department of Physics, Faculty of Science, Atatürk University, 25200 Erzurum, Turkey

Introduction

Nano-semiconductor-based dye-sensitized solar cells (DSSCs) are one of the most attractive photovoltaic devices due to good cost to performance ratio, short payback time, abundance of constituent materials, and less temperature dependence (O'Regan and Gratzel 1991). Even though DSSCs exhibit important economic and environmental advantages compared to the first- and second-generation photovoltaic devices, there are still some challenges preventing for their commercialization (Jung and Lee 2013). One of the most important reasons for this is the low efficiencies of the used photoanode structures which is the important part of the DSSCs. Mostly used photo-anode material in DSSCs is TiO_2 due to its superior photo-electrochemical performance, high electron injection efficiency, high stability, low cost, and low environmental impact (Kalowekamo and Baker 2009; Unold and Schock 2011; Gong et al. 2017; Chandiran et al. 2014; Jiang et al. 2016; Kilic et al. 2016a, b; Kilic and Turkdogan 2017; Turkdogan and Kilic 2017). However,

there are some disadvantages of TiO_2 as it exhibits a low electron transport rate and reduced photocatalytic efficiency owing to its fast electron-hole pair recombination rate (Zhang et al. 2009; Quintana et al. 2006). To accomplish these disadvantages, many different semiconductor materials have been used as photoanode such as ZnO and SnO_2. One of the mostly interested photoanode alternatives by the community is ZnO which typically offers increased surface area, reduced recombination rate, and high electron transport efficiency unlikely to TiO_2 (Bae et al. 2003). ZnO has been investigated as one of the most promising semiconductor materials for years due to its direct wide band gap energy (3.37 eV), large exciton-binding energy (60 meV), huge magneto-optic effect, high breakdown strength, and high infrared reflectivity (Ozgur et al. 2005). However, expected higher efficiency in DSSCs based on ZnO photoanode compared to that of TiO_2-based devices has not been yet achieved. The reason is mostly attributed to the instability of ZnO in acid dyes and its low electron injection efficiency (Chandiran et al. 2014). To overcome the low efficiency problem of the ZnO-based DSSCs, one of the methods used is to employ composite photoanode structures. One of the mostly used composite structures of ZnO/TiO_2 has been investigated with many research groups with the different forms (Yan et al. 2012; Wang et al. 2011; Milan et al. 2015; Turkdogan and Kilic 2017). ZnO/TiO_2 composite films prepared by screen printing method have been used as the photoanode in DSSCs, and the maximum of 1.87% power conversion efficiency (PCE) has been reported (Yan et al. 2012). Instead of using thin film structures of ZnO/TiO_2, nanoparticle composite photoanode structure has given rise to 4.52% PCE (Wang et al. 2011). Very recently, TiO_2 nanoparticle/ZnO nanofiber composite nanostructured photoanode has shown a one of the highest PCE around 6.54% (Milan et al. 2015). There are also a limited number of studies for the alternative composite structures together with ZnO in the literature. An example of ZnO/SnO_2 multilayer photoanode structure has indicated PCE of 4.96% structure (Yang et al. 2017).

In this study, the performance of the alternative composite photoanode of ZnO nanowire/CuO nanorods has been investigated in DSSCs to overcome the low conversion efficiency problem of ZnO in DSSCs. Also, optical, morphological, and structural as well as the chemical properties of the resulting ZnO/CuO hybrid structures were investigated in detail. Relatively high PCE of 6.18% was obtained compared to that of bare ZnO photoanode which might open up the usage of CuO composite structures as a photoanode layer in DSSCs.

Experimental procedure

Materials

A DSSC consists of five main components as follows: (1) transparent conductive substrate (TCO–FTO: fluorine-doped tin oxide or ITO: indium tin oxide); (2) n-type semiconductor layer; (3) dye molecules adsorbed on the surface of the semiconductor; (4) a liquid electrolyte containing a redox mediator; (5) Pt as a counter electrode capable of regenerating the redox mediator. In this study, commercial ITO-coated glasses having a sheet resistance of ~ 12 Ω /cm^2 were used as a substrate. First, the substrates were cleaned carefully by dipping them for 2 min in propan-2-ol, de-ionized water, methanol, and de-ionized water, in a sequence. The ITO substrates were cut into 2 cm × 2 cm pieces and ultrasonically cleaned with trichloroethylene, acetone, methanol, and deionized water. $CuCl_2.H_2O$ and $Zn(NO_3)_2{\cdot}6H_2O$ (aq) were used for the hydrothermal synthesis of the hybrid photoanode materials. A concentrated solution of ammonia (28%, Sigma-Aldrich) was used to adjust the pH of the hydrothermal reaction mixture. For the fabrication of DSSCs, iodine (I_2) (99.99%, Superpur1, Merck), lithium iodide (LiI; Merck), acetyl acetone (acac; Merck), and cis bis (isothiocyanato)bis(2,20-bipyridyl- 4,40-dicarboxylato)-ruthenium(II)bis tetrabutyl ammonium (N719) were used as received. Pt:ITO was used as the counter electrode for the DSSCs.

Synthesis of 1D-ZnO nanowire/CuO nanorod hybrid nanostructures for photoanode

The 1D-ZnO nanowire/CuO nanorod hybrid nanostructures were fabricated in two steps: (1) formation of ZnO NW structures on the ITO substrate, (2) growth of highly ordered CuO nanorods on the ZnO nanowires. ZnO nanowires were prepared by a hydrothermal method using varying molar ratios of ZnO, deposition time, pH, and reaction temperature. 0.15 g $Zn(NO_3)_2.4H_2O$ and 50 ml deionized water were mixed using a magnetic stirrer. Four milliliters ammonia (28%) was added to

adjust the pH ~ 11 of the solution. The solution was placed into a teflon-lined stainless steel autoclave. The ITO substrates were immersed into the solution, and the autoclave was then sealed and heated to 150 °C for 24 h. After a given growth time, the ZnO nanowire-coated samples were obtained. Those materials were dried under a flow of N_2 and then annealed in a furnace at 350 °C in ambient atmosphere for 40 min to form the DSSC photoanodes. Similarly, CuO nanorods were grown on ZnO NW substrates in a second step of experimental procedure. 0.52 g $CuCl_2.H_2O$ and 50 ml deionized water solution were mixed under continuous magnetic stirring and its pH was adjusted to ~ 11 by addition of ammonia solution. The ZnO nanowire substrates were immersed in the solution and then heated to 150 °C for 24 h. After the growth step, the substrates were dried under a flow of N_2 and were then annealed in a furnace at 350 °C in air for 30 min to form the hybrid structures.

Characterization of ZnO NW/CuO nanorod hybrid nanostructure thin films

The surface morphology of the nanostructures on each prepared sample was analyzed by scanning electron microscopy and energy-dispersive X-ray spectroscopy (SEM-EDAX) using a Philips XL30 ESEM-FEG/EDAX system. Crystal structure analysis was carried out using X-ray diffraction (XRD; Rigaku D/Max-IIIC diffractometer) with 1.54 Å Cu-Kα radiation and a 2θ range of 20–80°. Absorption measurements were carried out using a Perkin-Elmer UV-VIS Lambda 2S spectrometer. The PL measurements were conducted with the RF 5301 PC Shimadzu spectrofluorometer at room temperature. The surface composition of the samples was investigated using X-ray photoelectron spectroscopy (XPS; FlexMod-Specs), which is capable of providing atomic and molecular information on the surfaces of materials. The energy band alignment between ZnO and CuO was determined using interface experiments by stepwise deposition of the CuO on top of ZnO, and after each deposition step, the sample is analyzed via XPS. The energy band alignment at the ZnO/CuO interfaces was obtained from the core level binding energies using the Kraut method (Grant et al. 1978). It is known that the distance between the valence band maximum and the core-levels is constant for a material. This approach makes it possible to follow the evolution of the valence band maxima of the ZnO and the CuO as a function of film thickness. The Raman scattering measurements were taken using a micro Raman Witec Alpha 300R system with an excitation source of 514.5 nm at room temperature.

Device fabrication

Hybrid DSSCs based on ZnO NWs/CuO nanorod photoanode were prepared by adsorption of cisbis (isothiocyanato) bis (2,20-bipyridyl-4,40-dicarboxylato)-ruthenium (II) bis tetrabutyl ammonium (N719) dye molecules onto the surfaces of the prepared photoanodes for 6 h. The substrates were heated to 100 °C for 30 min before immersion in a 0.5-mM solution of the N719 dye. After 6 h, the samples were taken out, rinsed with acetonitrile, and dried with nitrogen gas. The photoanode and Pt:ITO counter electrode were sealed using a 20-μm polypropylene spacer and pressed together with binder clips. The electrolyte, which consists of 0.5 M tetra butyl ammonium iodide, 0.05 M I_2, and 0.5 M 4-tertbutylpyridine in acetonitrile, was introduced between the electrodes using capillary action. The active area was typically 0.25 cm^2. Photocurrent density versus voltage (J-V) data was recorded using a Keithley 175A digital multimeter using a 0.01-V/s voltage ramp rate under AM 1.5G solar simulator. The light source was a 250-W tungsten halogen lamp calibrated to irradiate the samples at 100 mW/cm^2 using a radiometer (IL1700, International). The external quantum efficiency (EQE) was measured with a spectral resolution of 5 nm using a 300 W xenon lamp.

Results and discussion

Morphological, structural, and optical properties of ZnO NW/CuO nanorod hybrid structures

SEM images in Fig. 1a–c show the surface morphology of the ZnO NWs, CuO nanorods, and CuO nanorods grown on the ZnO NW hybrid structure. Figure 1a shows the single-layer ZnO NWs grown on the glass substrate. High density and homogeneous distribution of ZnO NWs can be seen. The average diameter of the ZnO NWs has been found in the range of 40–50 nm, and the lengths are several tens of microns. Figure 1b presents the SEM image of the single-layer CuO nanorods. CuO nanorod is well covered on the substrate, and a good contact between the structures and substrate was achieved which is very important for electrical

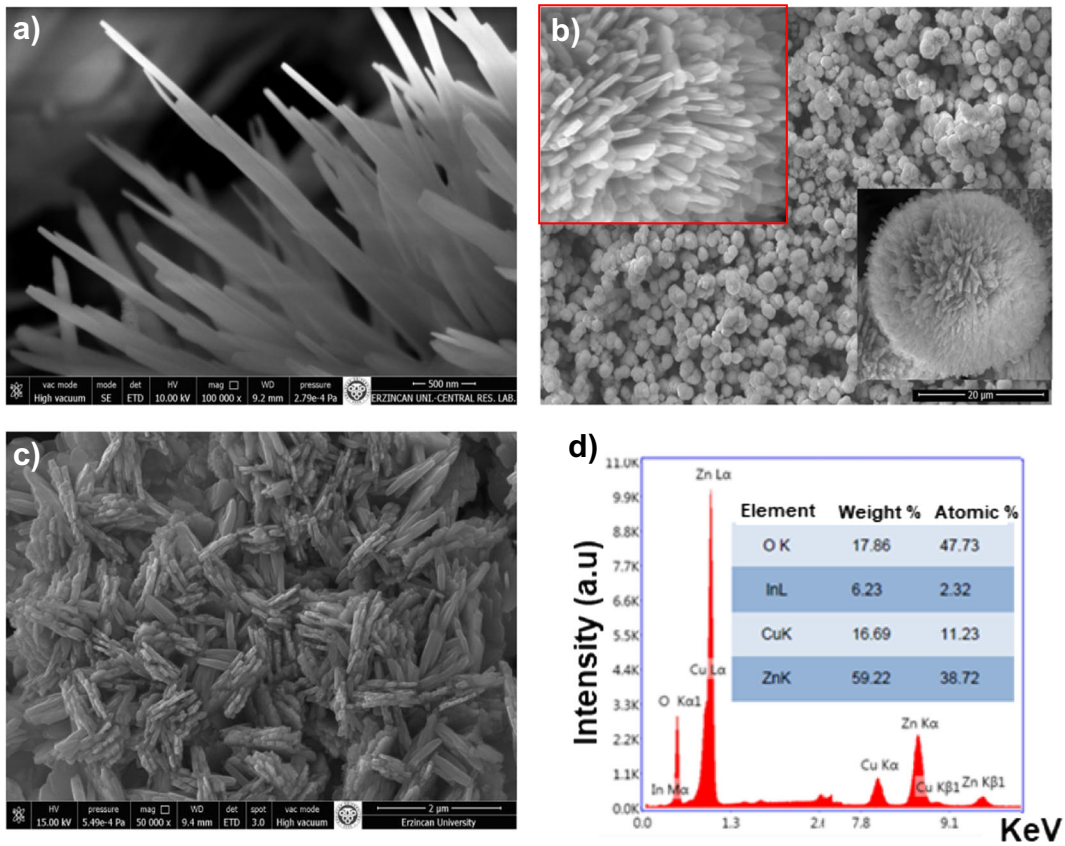

Fig. 1 SEM images of **a** ZnO nanowires, **b** CuO nanorods, **c** ZnO/CuO hybrid structures, **d** EDAX measurements of ZnO/CuO hybrid films

conduction pathway. The diameter of nanorods ranges from 20 to 50 nm and the length is up to 2 μm. These nanorods might lead to a high surface area which may help to enhance dye adsorption on the photoanode. As seen from Fig. 1c, hybrid nanostructures have been homogenously grown on the substrate by the hydrothermal method. As seen in the figure, the morphology of the hybrid structures is no more similar to either CuO nanorods or the ZnO NWs. This shows that the CuO nanorods were successfully and uniformly grown on the ZnO materials by the hydrothermal reaction and formed a hybrid film consisting of ZnO nanowires and CuO nanorods. EDAX analysis was carried out to determine the elemental compositions of the ZnO NWs/CuO nanorods hybrid films (Fig. 1d). Zn, Cu, and O peaks can be clearly seen from EDAX measurements. This data clearly indicates the formation of the ZnO/CuO hybrid structures, since the X-ray signals come from a few micrometers deep of the investigated sample.

In order to show the properties of the formed hybrid structures, series of analysis methods were employed. One of the employed analyses is to figure out the crystal structure of the materials by X-ray diffractometer. Figure 2a shows the XRD patterns of the as-synthesized ZnO/CuO hybrid structures. XRD peaks corresponding to both ZnO and CuO phases have been observed. The XRD pattern confirmed that CuO nanorods were successfully grown on ZnO nanowire structures with the acceptable crystal quality. All of the diffraction peaks were consistent with those of JCPDS card No. 48-1548, indicating that ZnO NWs have a pure hexagonal structure, while CuO nanorods show cupric phase with monoclinic system (space group of C2/c). The peaks at $2\theta \approx 36.23°$ belong to (101) planes of ZnO which is the dominant phase for ZnO. The diffraction peaks at 33.73^0, 39.92^0, and 49.42^0 are assigned to CuO (110), (200), and (− 202), respectively. Figure 2b presents the Raman spectra of ZnO/CuO hybrid samples. There are three Raman peaks assigned to the CuO at wavenumbers of 280, 332, and 632 cm^{-1}. In comparison with the vibrational spectra of bulk CuO, the peak at 280 cm^{-1} in CuO is assigned to the Ag and the peaks at

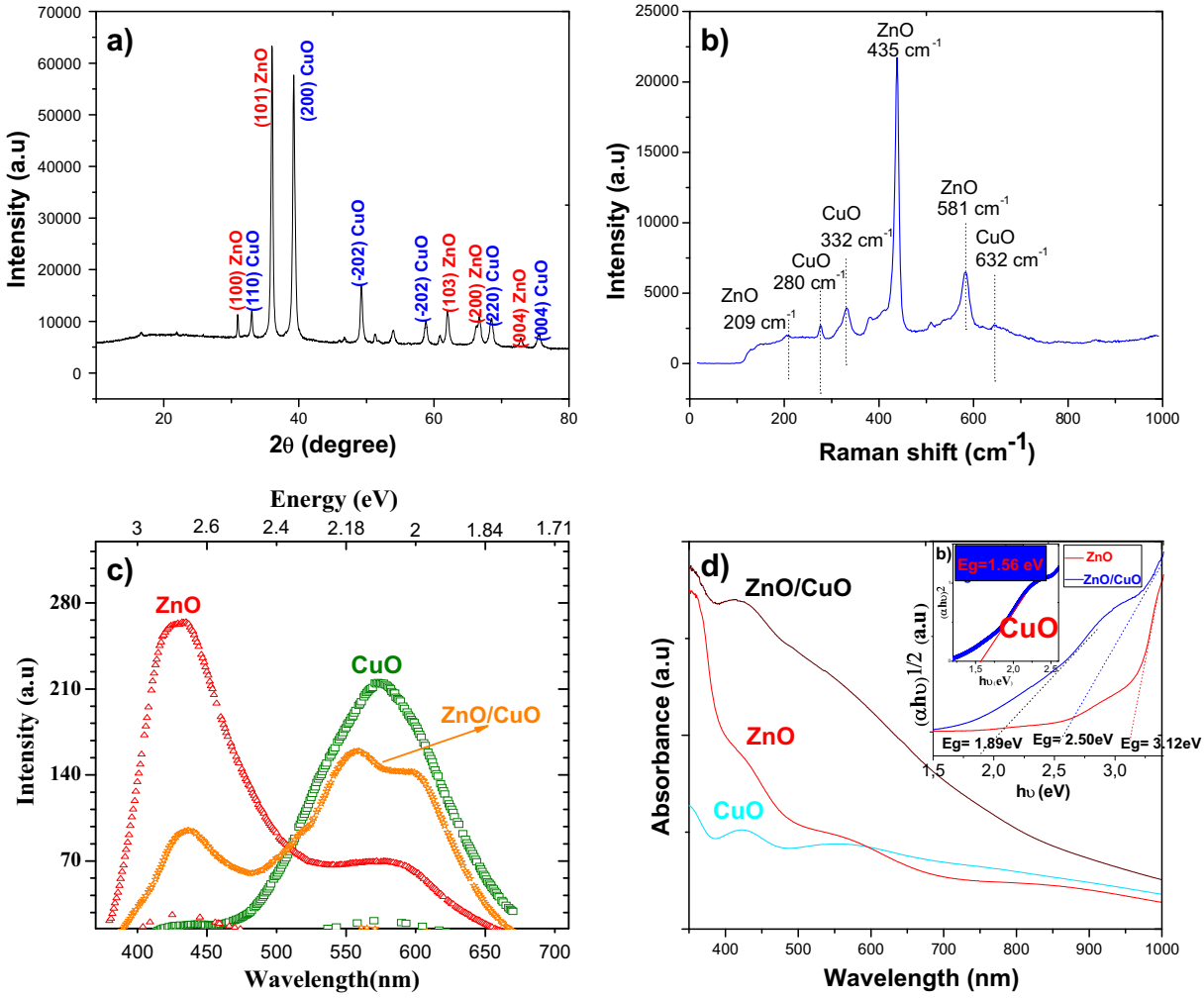

Fig. 2 Structural and optical characterization of ZnO/CuO hybrid films. **a** XRD characterization, **b** Raman spectra, **c** PL measurements, **d** Absorbance spectra and absorption coefficient/energy plots for the films of ZnO, CuO, and ZnO/CuO hybrid structures at room temperature

332 and 632 cm^{-1} to the Bg modes. A_1, E_1, and E_2 modes are Raman active and B_1 is forbidden in ZnO semiconductor. A dominant and strong intensity peak at 435 cm^{-1} indicates the spectrum known as the optical phonon, E_2. The E_2 mode, which is sensitive to the structural quality of the material, corresponds to the band characteristic for the wurtzite hexagonal phase of ZnO, which is also one of the characteristics of ZnO nanostructures (Umar et al. 2005). However, extra Raman band at 581 cm^{-1}, known to be related to the E_1 mode because of the oxygen deficiency (Wu and Liu 2002; Naseri et al. 2017), indicates the presence of oxygen vacancies in the ZnO nanostructures. Raman spectra confirm that both ZnO and CuO hybrid structures successfully grown with high structural quality on the glass substrate. The room temperature photoluminescence (PL) of ZnO NWs, CuO nanorods, and ZnO/CuO hybrid structures is shown in Fig. 2c. As seen in the figure, 1D-ZnO nanowire samples show near band edge emissions and broad deep level emission. These emissions are centered at 430 and 580 nm, respectively, as shown in the figure. The higher intensity of the near band-edge emission compared to that of deep level emission depicts the optical quality of the ZnO NWs. For the copper oxide, PL spectrum shows broad band centered at 600 nm. The observed broad band emission might be due to the combination of the near band edge emission and the deep level emissions. PL spectrum of ZnO/CuO hybrid nanostructures shows three-emission band at 430, 550, and 600 nm which

are the emissions combined with ZnO NWs and CuO nanorods. One of the most important properties of the photoanodes is their absorption properties. Absorption properties of ZnO NWs, CuO nanorods, and ZnO/CuO hybrid nanostructure were investigated by means of UV-VIS spectroscopy. Figure 2d shows the raw absorption data of the samples. As shown in the figure, ZnO/CuO hybrid structures absorb more photons in the whole visible and ultraviolet regions compared to that of bare ZnO NWs and CuO nanorods. In order to find out the band gap energy values of the samples, absorption spectrums are transferred into the absorption coefficients to draw well-known Tauc plots (Chi et al. 2012; Ghobadi 2013). Bandgap energy values of the samples were determined by intercepting the extrapolated linear region of the Tauc plots with "hv" axis. As seen in Fig. 2d, CuO and ZnO NWs have the bandgap energy values of 1.56 and 3.12 eV, respectively, and those values are in a good agreement with the literature (Orel et al. 1993; Ozgur et al. 2005). On the other hand, ZnO/CuO hybrid structures have shown two different fit regions as seen in the figure. Values of these two band gap energies are 1.89 and 2.50 eV. These bandgap values might belong to observe two different separated phases, namely CuO and ZnO, as also confirmed by the XRD, PL, and Raman measurements. However, the observed bandgap value for the ZnO, 2.50 eV, seems lowered which might be due to the combined band edge of CuO and ZnO deep level emission absorption spectra. It might be also speculated that, there is a chance of Cu incorporation into ZnO and this might be the reason lowering the bandgap energy and two different values might be possible.

XPS is a very important technique for analyzing chemical composition of elements on the surface. The detailed XPS analysis confirmed the formation of ZnO/CuO hybrid structures, which are shown in Fig. 3a. As seen in the figure, both Zn- and Cu-related peaks have been observed. High-resolution spectrum of the Cu element can be seen in Fig. 3b. The peaks observed at 933.7 and 954.8 eV confirmed the presence of Cu $2p_{3/2}$ and Cu $2p_{1/2}$ peaks, respectively. There are also satellite peaks observed in the spectrum which belong to the Cu^{+2} oxidation states confirming the formation of CuO. This is also consistent with the XRD data. The main peak at 933.7 eV is also characteristic of CuO (Cu^{2+}). High-resolution spectrum of the Zn has been indicated in Fig. 3c. The XPS peaks with binding energies of 1023.67 and 1045.79 eV correspond to Zn $2p_{3/2}$ and Zn $2p_{1/2}$, respectively. The detailed XPS analysis of O1s is shown in Fig. 3d. The figure also includes the deconvolution performed for the O1s spectrum. Two peaks have been realized as seen in the figure. The main peak at 529.2 eV corresponds to O 1s of CuO and the high energy peak at 531.30 eV is the characteristics of ZnO. O 1s peak with binding energy 529.2 eV represents bonding between O_2^- ions and Zn/Cu. The elemental percentages by using the deconvoluted O 1s spectrum, it is concluded that the O 1s sub-peak at 529.2 eV gives rise to 65% of the total spectral area confirming higher Cu–O percentages than the ZnO. The sub-peak at 531.30 eV might be due to O_2^- ions in oxygen deficient regions and/or adsorption of H_2O or O_2 molecules (Grant et al. 1978; Morasch et al. 2016).

Photovoltaic performance of ZnO/CuO hybrid structures

The design of hybrid DSSC structures used in this research is schematically shown in Fig. 4a and charge transfer processes of dye sensitized solar cell based on ZnO/CuO hybrid structures are illustrated in Fig. 4b. Under simulated solar irradiation, the dye molecules adsorbed on the n-type semiconductor film surface are excited from the ground state to the excited state, and the electron transferred to the lowest unoccupied molecular orbital (LUMO) of the dye is injected into the conduction band (CB) of the typical n-type semiconductor. The electron is transported through the semiconductor layer and then the external circuit to the counter electrode of the DSSC. The electron at the CB of the semiconductor may undergo recombination with the oxidized dyes and the redox couple mediator and this reduces the power conversion efficiency of the cells therefore this process is unfavorable and should be prevented to collect as much as electron possible to increase the PCE of the cells. In this study, CuO nanorods were coated on top of ZnO nanowire photoelectrode to form a barrier layer. It is expected that the hybrid structures have the potential to decrease the chance of electron-hole recombination. The growth of CuO nanorods on ZnO nanowires can effectively obstruct the injected electron from back-transferring the conduction band of the ZnO to the electrolyte. Consequently, the recombination of photo-generated electron with oxidized dye molecules or tri-iodide in the electrolyte is decreased. Photo-generated electrons in the CuO nanorods can rapidly inject into the conduction band of ZnO owing to decent bandgap

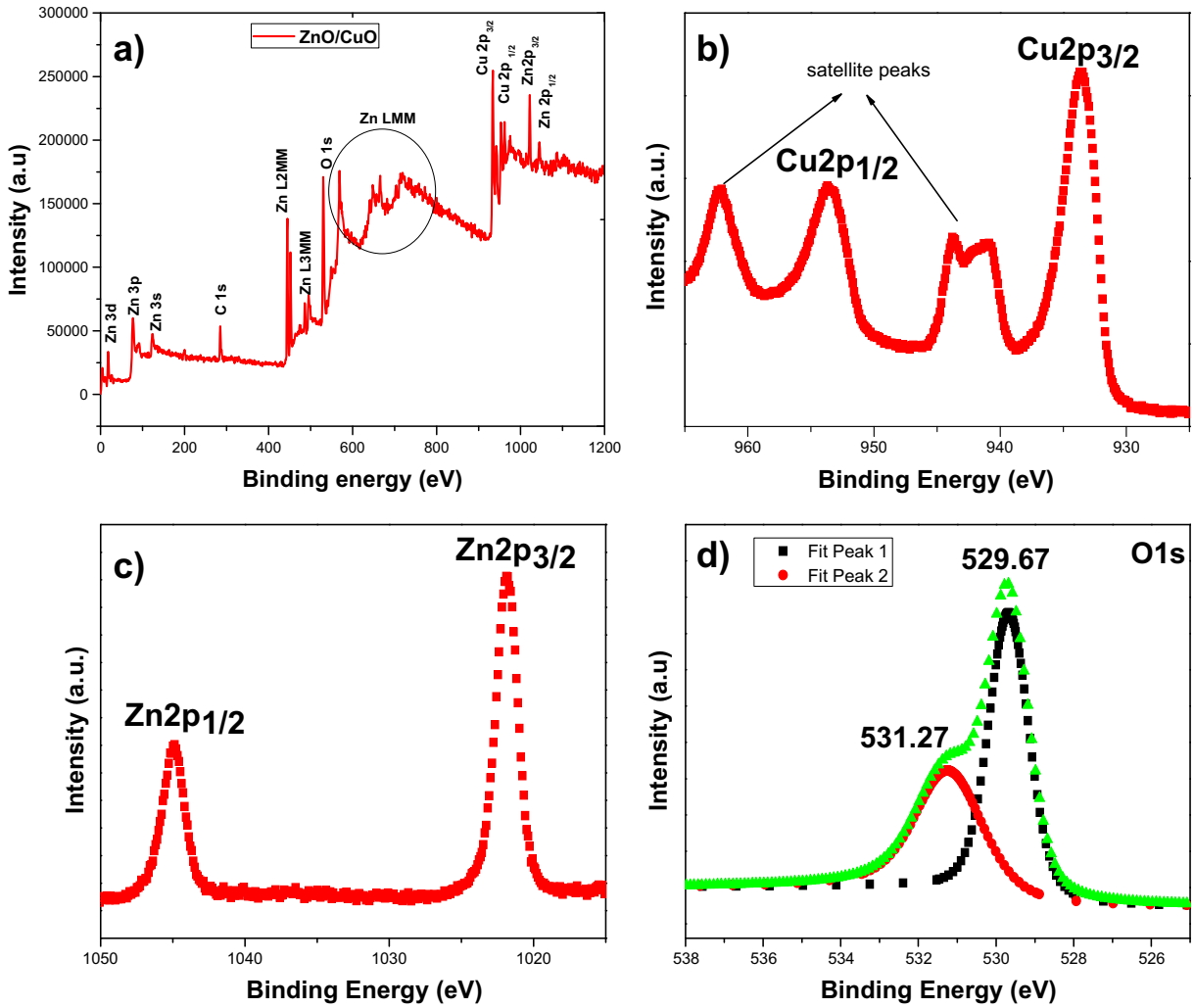

Fig. 3 XPS spectra of ZnO/CuO hybrid structures: **a** wide scan range of hybrid structures, **b** narrow scan of Cu 2p level peak, **c** Zn 2p level peak, **d** O 1s level peak

alignment between ZnO and CuO hybrid structures. CuO nanorods can form an inherent barrier layer between the photoelectrode and the electrolyte interface, which decreases the rate of electron recombination.

Figure 4c shows a comparison of the current density-voltage (J-V) characteristics of the ZnO/CuO hybrid structures and n-type ZnO nanowires. The corresponding photovoltaic parameters of the solar cells are summarized in Table 1.The dye-sensitized solar cells made from ZnO nanowires reached a promising level, $\eta =$ 5.05, %, $J_{sc} = 14.47$ mA cm^{-2}, $V_{oc} = 0.719$ V, and FF = 48.6%, using the N719 dye under an irradiance of 100 W cm^{-2}. The power conversion efficiency, short-circuit current density (J_{sc}), and open circuit voltage (Voc) of ZnO/CuO hybrid photoanodes have been measured around 6.18%, 14.76 mA cm^{-2}, and0.764 V, respectively, much higher than (~22.3, 2, and 6.25%, respectively) pure ZnO nanowire solar cell. Apparently, the CuO nanorods might have contributed to increase the electron diffusion length in the cells by providing a direct transport pathway from the point of electron injection to the ZnO substrate of the collection electrode. The light-scattering effect of the CuO nanorods onto the ZnO nanowire support likely enhanced the light-harvesting efficiency of the cell by increasing the optical length serving as a light-scattering center, which resulted in the enhanced J_{sc} observed for the hybrid film-based cell. As a result, it can be confirmed that the proposed ZnO/CuO hybrid films are very important to facilitate electron transport and light harvesting to

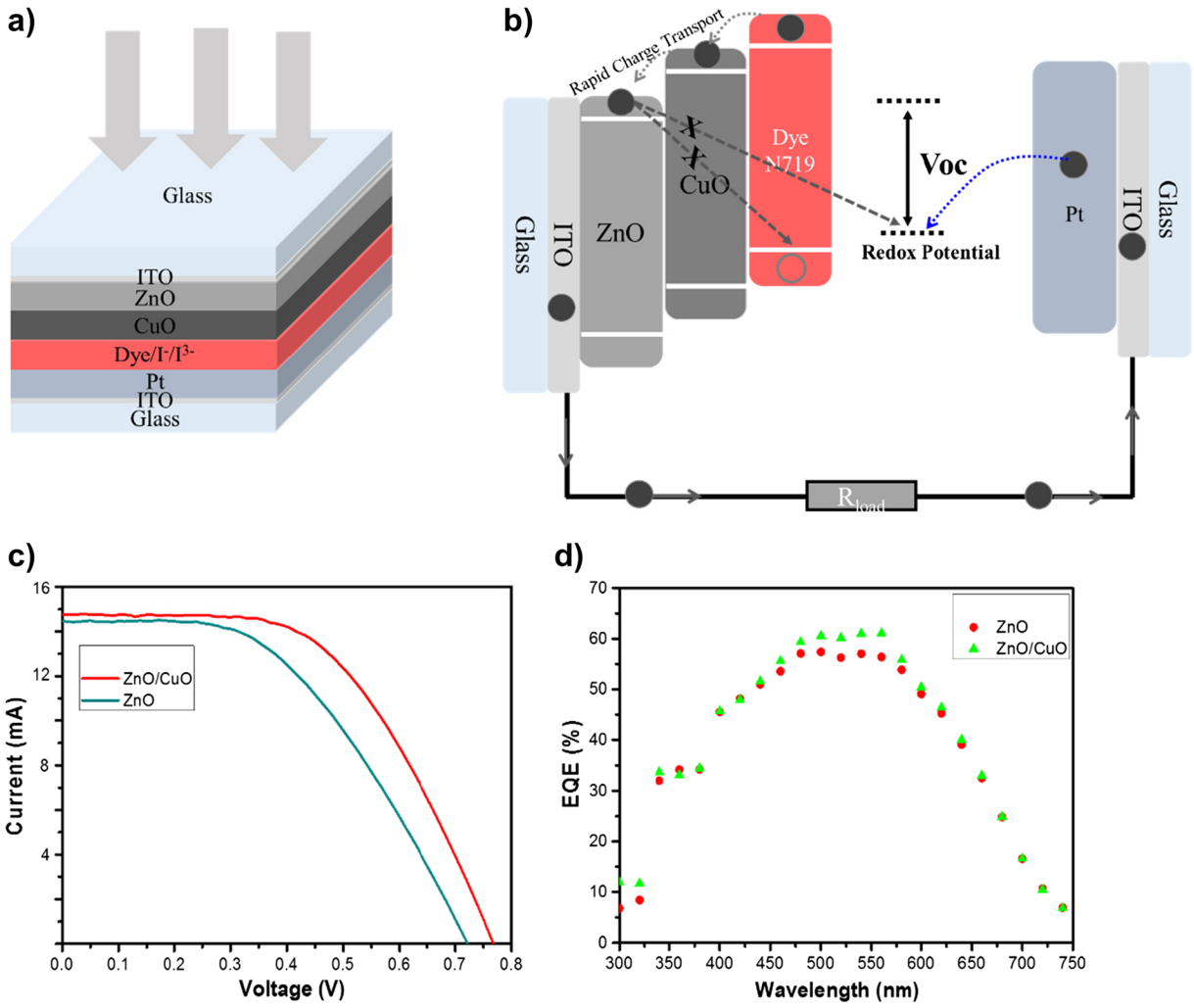

Fig. 4 **a** Schematic diagram of DSSC for ZnO/CuO hybrid structures. **b** Band structures of the device and aligned bands where we can see the carrier generation and its transportation to flow current through the load. **c** Current density-voltage (J-V) characteristics of dye-sensitized solar cells loaded with N719 dye and 0.25 cm^2 active surface area measured under AM 1.5G solar irradiance (100 mW cm^{-2}). **d** EQE spectra of the cells

enhance the solar conversion efficiency of DSSCs. The external quantum efficiency (EQE) of the ZnO/CuO hybrid films has been evaluated using their incident photon-to-current conversion efficiency (IPCE or QE) spectra. The observed improved EQE can be explained by the increased light capture efficiency, electron injection, and collection efficiency of the films. Figure 4d shows the EQE spectra of the DSSCs with ZnO nanowires and ZnO/CuO hybrid photoelectrodes as a function of the illumination wavelength. The EQE at around 550 nm overlaps with the maximum absorption wavelength of the N719 dye. The EQE of the ZnO/CuO hybrid films was higher than that of the bare ZnO film within the entire wavelength region investigated. These observed enhancements in QE mainly arose from the increased electron injection efficiency and light-harvesting efficiency of the films and were also attributed to the enhancement of dye loading resulting from

Table 1 Photovoltaic properties of DSSC based on ZnO/CuO hybrid photoanode nanostructures. Measurements were performed under AM 1.5G one sun (light density, 100 mW cm^{-2}). The active area was set at 0.25 cm^2 for all of the cells

Sample	FF (%)	Voc (V)	Jsc (mA/cm^2)	(%)
ZnO	48.6	0.719	14.47	5.05
ZnO/CuO	54.8	0.764	14.76	6.18

the higher surface area of the hybrid films. The high dye absorption ability and EQE values confirmed that the introduced photons were effectively absorbed, resulting in larger J_{sc} and improved solar conversion efficiency.

Conclusion

CuO nanorods were grown on 1D ZnO NWs for application in hybrid-DSSCs with enhanced solar to power conversion efficiency. CuO nanorods on the ZnO nanowires were utilized as a blocking layer. Photocurrent measurements indicated that the light-harvesting efficiency of the obtained ZnO/CuO hybrid film was higher than that of bare ZnO nanostructures. Current density-voltage characterization indicated that the ZnO/CuO hybrid structures exhibit a remarkably enhanced power conversion efficiency of 6.18%, about 30% higher than that of pure ZnO nanowires. Our results show that ZnO/CuO hybrid structures are clearly favorable for DSSC applications owing to their fast electron transport, effective diffusion length, and reduced rate of charge recombination. We also show the growth mechanism of CuO nanorods on the ZnO nanowires and Raman, XPS, and XRD characterization results confirm the formation of ZnO/CuO hybrid structures. The optical measurements characterized CuO as a highly absorbing direct gap semiconductor. CuO band gap was measured to be 1.56 eV while ZnO/CuO hybrid structures have a 2.50-eV bandgap energy. Interface experiment of ZnO/CuO hybrid structures indicated that while the photocurrent density is believed to be generated by charge injection from CuO on top of ZnO NWs, ZnO NWs may also contribute to the photovoltage due to the high band bending induced by CuO deposition.

Compliance with ethical standards

Conflict of interest The authors declare that they have no conflict of interest.

References

Bae HS, Yoon MH, Kim JH, Im S (2003) Photodetecting properties of ZnO-based thin-film transistors. Appl Phys Lett 83(25):5313–5315. https://doi.org/10.1063/1.1633676

Chandiran AK, Abdi-Jalebi M, Nazeeruddin MK, Grätzel M (2014) Analysis of electron transfer properties of ZnO and TiO2 photoanodes for dye-sensitized solar cells. ACS Nano 8(3):2261–2268. https://doi.org/10.1021/nn405535j

Chi T, Cheng IC, Chen JZ (2012) Bandgap tuning of MgZnO in flexible transparent n+-ZnO: Al/n-MgZnO/p-CuAlO x: Ca diodes on polyethylene terephthalate substrates. J Alloys Compd 544:111–114. https://doi.org/10.1016/j.jallcom.2012.08.004

Ghobadi N (2013) Band gap determination using absorption spectrum fitting procedure. Int. Nano Lett 3(1):2. https://doi.org/10.1186/2228-5326-3-2

Gong J, Sumathy K, Qiao Q, Zhou Z (2017) Review on dye-sensitized solar cells (DSSCs): advanced techniques and research trends. Renew Sustain Energy Rev 68:234–246. https://doi.org/10.1016/j.rser.2016.09.097

Grant R, Waldrop J, Kraut E (1978) XPS measurements of abrupt Ge-GaAs heterojunction interfaces. J Vac Sci Technol 15(4):1451–1455. https://doi.org/10.1116/1.569806

Jiang Y, Yang Y, Qiang L, Ye T, Li L, Su T, Fan R (2016) Enhanced photovoltaic performance of dye-sensitized solar cells by the strategy of introducing copper (II) silico tungstate into photoanode and counter electrode. J Power Sources 327:465–464. https://doi.org/10.1016/j.jpowsour.2016.07.086

Jung HS, Lee JK (2013) Dye sensitized solar cells for economically viable photovoltaic systems. J Phys Chem Lett 4(10):1682–1693. https://doi.org/10.1021/jz400112n

Kalowekamo J, Baker E (2009) Estimating the manufacturing cost of purely organic solar cells. Sol Energy 83(8):1224–1231. https://doi.org/10.1016/j.solener.2009.02.003

Kilic B, Turkdogan S, Astam A, Ozer OC, Asgin M, Cebeci H, Urk D, Mucur SP (2016a) Preparation of carbon nanotube/TiO2 mesoporous hybrid photoanode with iron pyrite (FeS2) thin films counter electrodes for dye-sensitized solar cell. Sci Rep 6(1):27052. https://doi.org/10.1038/srep27052

Kilic B, Turkdogan S, Ozer OC, Asgin M, Bayrakli O, Surucu G, Astam A, Ekinci D (2016b) Produce of graphene/iron pyrite (FeS 2) thin films counter electrode for dye-sensitized solar cell. Mater Lett 185:584–587. https://doi.org/10.1016/j.matlet.2016.06.069

Kilic B, Turkdogan S (2017) Fabrication of dye-sensitized solar cells using graphene sandwiched 3D-ZnO nanostructures based photoanode and Pt-free pyrite counter electrode. Mater Lett 193:195–198. https://doi.org/10.1016/j.matlet.2017.01.128

Milan R, Selopal GS, Epifani M, Natile MM, Sberveglieri G, Vomiero A, Concina I (2015) ZnO@SnO2 engineered composite photoanodes for dye sensitized solar cells. Sci Rep 5(1):14523. https://doi.org/10.1038/srep14523

Morasch J, Wardenga HF, Jaegermann W, Klein A (2016) Influence of grain boundaries and interfaces on the electronic structure of polycrystalline CuO thin films. Phys Status Solidi A 213(6):1615–1624. https://doi.org/10.1002/pssa.201533018

Naseri A, Samadi M, Mahmoodi NM, Pourjavadi A, Mehdipour A, Moshfegh AZ (2017) Tuning composition of electrospun ZnO/CuO nanofibers: toward controllable and efficient solar photocatalytic degradation of organic pollutants. J Phys Chem C 121(6):3327–3338. https://doi.org/10.1021/acs.jpcc.6b10414

O'Regan B, Gratzel M (1991) A low cost, high-efficiency solar cell based on dye-sensitized colloidal TiO2 films. Nature 353(6346):737–739. https://doi.org/10.1038/353737a0

Orel B, Svegl F, Bukovec N, Kosec M (1993) Structural and optical characterization of CuO particulate solid films and the corresponding gels and xerogels. J Non-Cryst Solids 159(1-2):49–64. https://doi.org/10.1016/0022-3093(93)91281-7

Ozgur U, Alivov YI, Liu C, Teke A, Reshchikov MA, Dogan S, Avrutin V, Cho SJ, Morkoc H (2005) A comprehensive review of ZnO materials and devices. J Appl Phys 98(4): 41301. https://doi.org/10.1063/1.1992666

Quintana M, Edvinsson T, Hagfeldt A, Boschloo G (2006) Comparison of dye-sensitized ZnO and TiO2 solar cells: studies of charge transport and carrier lifetime. J Phys Chem C 111(2):1035–1041. https://doi.org/10.1021/jp065948f

Turkdogan S, Kilic B (2017) Metal oxide sandwiched dye-sensitized solar cells with enhanced power conversion efficiency fabricated by a facile and cost effective method. Mater Sci Semicond Process 71:382–388. https://doi.org/10.1016/j.mssp.2017.08.036

Umar A, Kim SH, Lee YS, Nahm KS, Hahn YB (2005) Catalyst-free large-quantity synthesis of ZnO nanorods by a vapor–solid growth mechanism: structural and optical properties. J Cryst Growth 282(1-2):131–136. https://doi.org/10.1016/j.jcrysgro.2005.04.095

Unold T, Schock HW (2011) Nonconventional (non-silicon-based) photovoltaic materials. Annu Rev Mater Res 41(1): 297–321. https://doi.org/10.1146/annurev-matsci-062910-100437

Wang M, Wang Y, Li J (2011) ZnO nanowire arrays coating on TiO2 nanoparticles as a composite photoanode for a high efficiency DSSC. Chem Commun 47(40):11246–11248. https://doi.org/10.1039/C1CC15310B

Wu JJ, Liu SC (2002) Catalyst-free growth and characterization of ZnO nanorods. JPhys Chem B 106(37):9546–9551. https://doi.org/10.1021/jp025969j

Yan LT, Wu FL, Peng L, Zhang LJ, Li PJ, Dou SY, Li TX (2012) Photoanode of dye-sensitized solar cells based on a ZnO/TiO2 composite film. Int J Photoenergy 2012:613969–613964. https://doi.org/10.1155/2012/613969

Yang M, Dong B, Yang X, Xiang W, Ye Z, Wang E, Wan L, Zhao L, Wang S (2017) TiO2 nanoparticle/nanofiber–ZnO photoanode for the enhancement of the efficiency of dye-sensitized solar cells. RSC Adv 7(66):41738–41744. https://doi.org/10.1039/c7ra07644d

Zhang Q, Dandeneau CS, Zhou X, Cao G (2009) ZnO nanostructures for dye-sensitized solar cells. Adv Mater 21(41):4087–4108. https://doi.org/10.1002/adma.200803827